On the Impact of Different Mapping Functions on Geodetic and Tropospheric Products from VLBI Data Analysis

Kyriakos Balidakis[1], Florian Zus[2], Jan Douša[3], Tobias Nilsson[2], Susanne Glaser[1], Benedikt Soja[2], Maria Karbon[2], Robert Heinkelmann[2], Harald Schuh[1,2]

Abstract We assess the impact of mapping functions on geodetic very long baseline interferometry (VLBI). The results from the analysis of 13 years of VLBI data processed by employing different mapping functions are intercompared. One of these is the newly developed Potsdam mapping function (PMF). The PMF performs slightly better than the VMF1 in terms of baseline length repeatability and Earth orientation parameters. Additionally, we investigated the impact of the underlying spatial resolution of the numerical weather model employed for the ray-tracing on the geodetic estimates, and we found millimeter level differences in the height estimates during severe weather events.

Keywords VLBI, troposphere, mapping functions, ray-tracing, Earth orientation parameters

1 Introduction

In data analysis of space geodetic techniques, such as Very Long Baseline Interferometry (VLBI) and Global Navigation Satellite Systems (GNSS), including observations spanning a wide range of elevations improves the de-correlation of the estimated position height from the estimates of the residual zenith delay and the clock parameters, hence enhancing the precision of these parameters. Unlike low elevation GNSS observations, the VLBI observations are unaffected by the effects of multi-path scattering and phase center variations. Thus the adoption of an elevation dependent weighting strategy as well as an elevation mask angle ($\approx 7^\circ$) is inessential. This allows VLBI analysis to benefit from fully utilizing low elevation observations. Nevertheless, as the elevation angle decreases, the mapping function (MF) uncertainties rapidly increase, degrading the positioning precision. Therefore, it is imperative that accurate mapping functions be applied and that their uncertainties be described stochastically in the adjustment.

Throughout the years, several tropospheric MF have been developed --- the interested reader is referred to Nilsson et al. (2013) for a review. To date, the most accurate and widely globally applied MF are the Vienna Mapping Functions 1 (VMF1) (Böhm et al., 2006), because the functional formulation and the underlying data set (ECMWF operational analysis) are very accurate. Therefore, they are recommended by the latest IERS Conventions (Petit and Luzum, 2010). However, the climatological approach adopted for the description of coefficients b and c prevents parametrized mapping from representing short-term and anomalistic atmospheric behavior (cf. Section 2). In addition to this, as the underlying numerical weather model (NWM) is intended to produce the best state estimate, it is subject to system changes (e. g., February 2006, January 2010, and March 2016) which consequently lead to inhomogeneities in the time series of the products. In an effort to address these issues, we used our in-house ray-trace software package (Zus et al., 2012) to determine the a, b, and c coefficients utilizing the ERA-Interim reanalysis (Dee et al., 2011). Hereinafter, this rigorous MF will be referred to as the PMF.

In this paper, we study the benefit of applying the PMF in VLBI analysis. Section 2 outlines the develop-

1. Technische Universität Berlin, Institute of Geodesy and Geoinformation Science, Berlin, Germany
2. Helmholtz Centre Potsdam, GFZ German Research Centre for Geosciences, Space Geodetic Techniques, Potsdam, Germany
3. Geodetic Observatory Pecný of the Research Institute of Geodesy, Topography and Cartography, Czech Republic

ment of the PMF. In Section 3, we perform a series of VLBI solutions and elaborate on the geodetic results. Section 4 recapitulates the results and provides an outlook.

2 The Potsdam Mapping Functions (PMF)

In essence, the total delay that radio signals experience when traversing the neutral atmosphere is approximated as a function of elevation ε and azimuth α:

$$\begin{aligned}\tau_{trop}(\varepsilon,\alpha) = {} & mf_h d_h^z + mf_w d_w^z \\ & + mf_g(G_{NS}\cos(\alpha) + G_{EW}\sin(\alpha))\end{aligned} \tag{1}$$

where the subscript h stands for hydrostatic and w for wet. The zenith delays are denoted by d_i^z, and G_{NS} and G_{EW} are the total linear horizontal delay gradients. The fitting ansatz for both symmetric MF (mf_i) follows the continued fraction form normalized to yield unity at zenith (Herring, 1992). Here, the total gradient MF mf_g follows Chen and Herring (1997).

$$mf_i = \begin{cases} \dfrac{1+\dfrac{a_i}{1+\dfrac{b_i}{1+c_i}}}{\sin(\varepsilon)+\dfrac{a_i}{\sin(\varepsilon)+\dfrac{b_i}{\sin(\varepsilon)+c_i}}}, & \text{for } i = h \vee w \\ \dfrac{1}{\sin(\varepsilon)\tan(\varepsilon)+0.0032}, & \text{for } i = g \end{cases} \tag{2}$$

For our investigations, we employ ERA-Interim at the original resolution (six-hourly $1^\circ \times 1^\circ$ fields on 60 model levels) and the ray-trace algorithm proposed by Zus et al. (2012). In essence, for the considered VLBI stations we compute tropospheric delays for various elevation and azimuth angles in order to estimate the a, b, and c coefficients of the MF and the total linear horizontal delay gradients by a least-squares fit. A detailed description can be found in Douša et al. (2016).

We compare our product (PMF_1.0 hereafter) with the original VMF1 (VIE-VMF1) and UNB-VMF1[1] (from NCEP reanalysis 1) in terms of slant total delays (STD) for $\varepsilon = 5^\circ$ (cf. Figure 1). Because differences in the MF coefficients are overshadowed by discrepancies in both hydrostatic and non-hydrostatic zenith delays between different providers, we follow Balidakis et al. (2016) to extract the necessary data for the calculation of the zenith delays. The rule of thumb suggests that the STD difference at the lowest elevation angle a station observed during a session equals approximately five times the expected estimated station height difference (Böhm, 2004). Considering the rather large bias present in the UNB-VMF1 differences, we have opted not to consider it in the subsequent VLBI analysis.

3 VLBI Data Analysis and Results

We perform two series of VLBI solutions. Initially, we utilize the classical Gauß-Markov least-squares adjustment module of the VieVS@GFZ VLBI software (Böhm et al., 2012; Nilsson et al., 2015) to analyze observations from the IVS-R1 and IVS-R4 sessions (1,326 24-hour multi-baseline sessions), spanning the period 2002-2015 and featuring in total a 32-station global network. We produce three solutions, varying only the MF applied: (1) VIE-VMF1, (2) GPT2w (Böhm et al., 2015), and (3) PMF_1.0.

To study sub-daily variations and the impact of the resolution of the underlying NWM on the geodetic results, the Kalman filter module of VieVS@GFZ is better suited (Soja et al., 2015). We analyze the best existing continuous VLBI data set, CONT14[2]. The filter is run forwards and backwards, followed by a smoother. We produce four solutions, with a solution employing PMF from ray-tracing in $0.5^\circ \times 0.5^\circ$ fields (PMF_0.5 hereafter) and another from ray-tracing in CMC-GDPS[3] (UNB-VMF1 hereafter), additionally to the above-listed MF, excluding GPT2w.

In all solutions we employ homogenized in situ data (Balidakis et al., 2016). In addition to the conventional displacement models (Petit and Luzum, 2010), we correct for deformations induced by non-tidal atmospheric pressure loading (NTAL[4]) and continental water storage loading (Dill and Dobslaw, 2013), to reduce correlations. Station coordinates and Earth orientation parame-

[1] `unb-vmf1.gge.unb.ca/About.html`

[2] Fifteen consecutive 24-hour sessions in May 2014, featuring a 17 station global network.

[3] `dd.weather.gc.ca/model_gem_global/25km`

[4] The NTAL series are calculated employing the operational model of ECMWF, utilizing MOG2D-G to describe the dynamic ocean response to pressure and wind forcing.

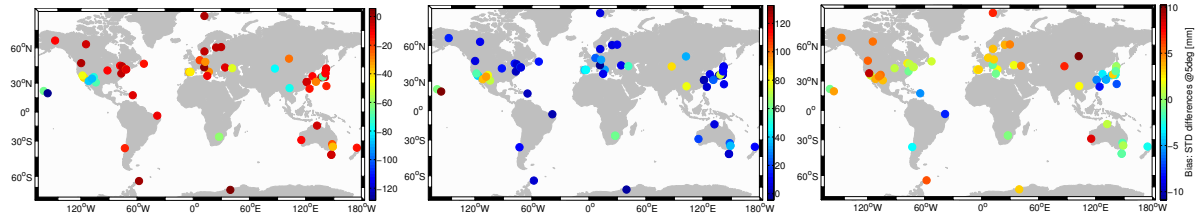

(a) UNB-VMF1 - VIE-VMF1 (b) PMF - UNB-VMF1 (c) PMF - VIE-VMF1

Fig. 1: Shown are the average STD differences in mm at $\varepsilon = 5^\circ$ between the VIE-VMF1, UNB-VMF1 and PMF_1.0, calculated from 14 years of data, utilizing the same zenith delays for all three cases.

ters (EOP) are estimated at 24-hourly intervals, whereas ZWD are estimated at hourly and linear horizontal delay gradients at six-hourly intervals.

In VLBI analysis, varying the MF mainly impacts the height coordinate component. We find that when the PMF_1.0 is applied instead of VIE-VMF1, the estimated height changes by more than 1 mm at only two sites, whereas GPT2w biases 35% of the sites considered, w. r. t. VIE-VMF1. The weighted root-mean-square (WRMS) differences between VIE-VMF1 and PMF_1.0 indicate marginal changes. When GPT2w is applied, the WRMS increase can be as large as 16% w. r. t. VIE-VMF1 (cf. Figure 2).

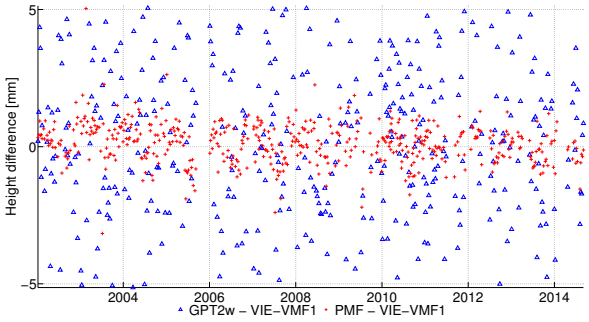

Fig. 2: Differences of the residual height estimates at Westford, USA, between the solutions applying VIE-VMF1, PMF_1.0, and GPT2w.

Figure 3 illustrates that in the presence of severe weather events, solutions obtained using MF that differ only in the resolution of the underlying NWM may diverge signficantly. In this example, there was a severe weather event at Tsukuba, Japan, on May 18, corresponding to day of year 138 in 2014.

Another quantitative measure of the impact of employing different MF on the geodetic results is provided

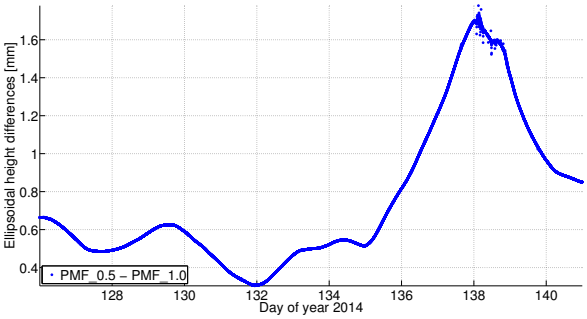

Fig. 3: Differences of the residual height estimates at Tsukuba, during CONT14, between the solutions applying PMF_1.0 and PMF_0.5.

by studying the changes in the baseline length repeatability. Therefore, we calculate the WRMS scatter of baseline length estimates. Given a baseline length time series $\{b\}_{i=1}^{N}$, the formula we used reads:

$$WRMS = \sqrt{\sum_{i=1}^{N} \frac{v_{b_i}^2}{\sigma_{v_{b_i}}^2} \Big/ \sum_{i=1}^{N} \frac{1}{\sigma_{v_{b_i}}^2}}, \qquad (3)$$

where v_{b_i} are the baseline length residuals from a straight-line fit solved by a rigorous evaluation of the non-linear Gauß-Helmert model and $\sigma_{v_{b_i}}$ are their formal errors. We find that PMF performs slightly better than VIE-VMF1 (for $\approx 60\%$ of baselines longer than 1,000 km), and improves the repeatability for $\approx 65\%$ of the baselines compared to GPT2w.

To assess the impact of varying the MF on the resulting terrestrial reference frame (TRF), the seven-parameter similarity transformation is performed, in a session-wise manner. Figure 4c portrays that the scale factor between the VIE-VMF1 and the PMF_1.0 solutions yields sub-mm changes. The slightly positive bias

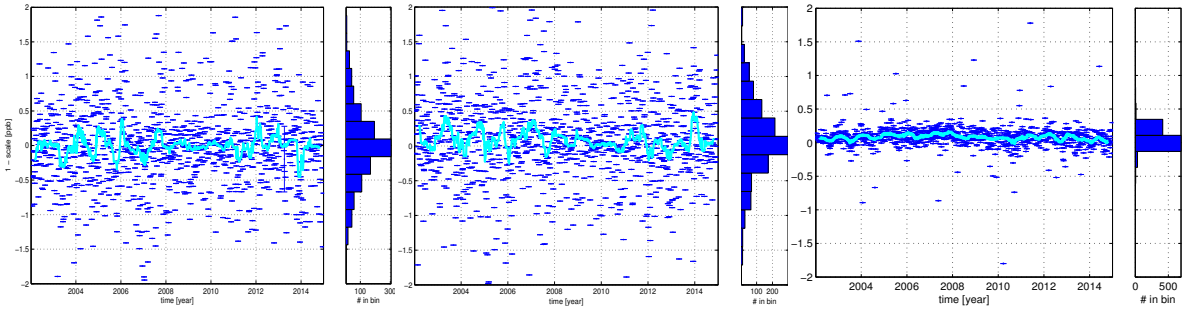

(a) GPT2w - PMF (b) VIE-VMF1 - GPT2w (c) VIE-VMF1 - PMF

Fig. 4: Time series of scale difference estimates from the epoch-wise Helmert transformation among all solutions are shown in blue (dark) ($1\,ppb \approx 6.4\,mm$). The cyan (light) line represents a 90-day moving median.

can be explained by (1) the different underlying NWM data, i. e., the ECMWF ERA-Interim reanalysis versus the ECMWF operational analysis, (2) the difference between a rigorous MF and a MF based on the VMF1 concept, (3) the differences in the underlying ray-trace algorithms, e. g., the PMF utilizes a local (Gaussian) curvature radius of the Earth whereas the VMF1 utilizes a constant curvature radius for the Earth, and finally (4) the different boundary conditions considered. On the contrary, Figures 4a and 4b demonstrate that using an empirical MF considerably distorts the scale at the cm-level, depending on weather conditions.

Differences between the MF tested here propagate rather moderately to the estimated EOP. Nevertheless, it has to be noted that the WRMS of all EOP series marginally increases when GPT2w is applied in lieu of VIE-VMF1. In particular, the WRMS of the polar motion components inflates by $\approx 2\,\%$, and an offset as large as $3\,\mu as$ and $-20\,\mu as$ ($\approx 1\,mm$ at a 10,000 km baseline) appears in x_{pole} and y_{pole}, respectively. Applying the PMF reduces the WRMS of the celestial pole offset x_{CIP} by $\approx 3.6\,\%$ compared to VIE-VMF1. The standard deviation in the time series of the differences of ZWD, NS, and EW gradients between the VIE-VMF1 solution and GPT2w, is 3, 2.8, and 2.7 times larger compared to the differences between PMF and the VIE-VMF1 solution (cf. Figure 5). An annual signal is visible in the differences between PMF and VIE-VMF1.

In Figure 6, the discrepancies in the estimated ZWD at Tsukuba during CONT14 are shown. The best agreement is found between PMF_0.5 and PMF_1.0, whereas the largest discrepancies lie between VIE-VMF1 and PMF_0.5 (e. g., the bias in the ZWD series of Fortaleza, Brazil exceeds 1 mm—not shown here).

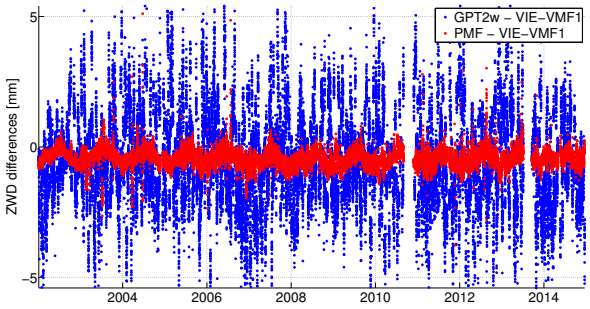

Fig. 5: The differences of the ZWD estimates at Wettzell, Germany, between the solutions applying VIE-VMF1, PMF_1.0, and GPT2w.

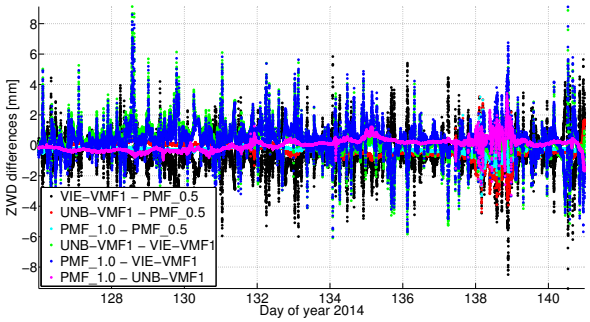

Fig. 6: The differences of the ZWD estimates at Tsukuba, during CONT14 between VIE-VMF1, UNB-VMF1, PMF_1.0, and PMF_0.5.

4 Conclusions and Outlook

In this study, we address the MF that are employed for VLBI data analysis. The PMF was developed from rigorous ray-tracing in ERA-Interim, based on the ad-

vanced mapping concept. Two series of VLBI solutions were generated employing the least-squares method and a Kalman filter, to study long and short term effects, respectively. Intercomparing the estimates, we find that the scale is distorted (up to the cm-level) when employing the empirical GPT2w model, whereas the differences between VIE-VMF1 and PMF are at the sub-mm level. PMF marginally improves the estimated EOP series and the baseline length repeatability compared to GPT2w and VIE-VMF1. For CONT14, mm-level differences in the height estimates can stem from the resolution of the underlying NWM used for the ray-tracing. A more thorough analysis spanning the entirety of VLBI data is foreseen.

Acknowledgements

We acknowledge the IVS (Schuh and Behrend, 2012) for coordinating the VLBI experiments analyzed in this study. DWD and ECMWF are acknowledged for granting access to the NWM data used in this study. Thalia Nikolaidou is acknowledged for providing data from ray-tracing in NCEP reanalysis 1 and CMC-GDPS. KB works under DFG project HE 5937/2-1.

References

Balidakis K, with seven co-authors (2016) On the impact of inhomogeneities in meteorological data on VLBI data analysis. In: Behrend D, Baver K, Armstrong K (eds), IVS 2016 General Meeting Proceedings, this volume.

Böhm J, Werl B, Schuh H (2006) Troposphere mapping functions for GPS and very long baseline interferometry from European Centre for Medium-Range Weather Forecasts operational analysis data. J Geophys Res Solid Earth 111(B2).

Böhm J (2004) Troposphärische Laufzeitverzögerungen in der VLBI. Geowissenschaftliche Mitteilungen, Geowissenschaftliche Mitteilungen 68.

Böhm J, with seven co-authors (2012) The New Vienna VLBI Software VieVS. In: Kenyon S, Pacino MC, Marti U (eds) Geodesy for Planet Earth, International Association of Geodesy Symposia, vol 136, Springer Berlin Heidelberg, pp 1007–1011.

Böhm J, Möller G, Schindelegger M, Pain G, Weber R (2015) Development of an improved empirical model for slant delays in the troposphere (GPT2w). GPS Solut 19(3):433–441.

Chen G, Herring TA (1997) Effects of atmospheric azimuthal asymmetry on the analysis of space geodetic data. J Geophys Res Solid Earth 102(B9):20,489–20,502

Dee DP, with 35 co-authors (2011) The ERA-Interim reanalysis: configuration and performance of the data assimilation system. Quarterly Journal of the Royal Meteorological Society 137(656):553–597.

Dill R, Dobslaw H (2013) Numerical simulations of global-scale high-resolution hydrological crustal deformations. J Geophys Res Solid Earth 118:5008–5017.

Douša J, with eight co-authors (2016) Benchmark campaign and case study episode in Central Europe for development and assessment of advanced GNSS tropospheric models and products. Atmos Meas Tech Discuss 2016:1–40.

Herring TA (1992) Modeling atmospheric delays in the analysis of space geodetic data. In: De Munck JC, Spoelstra TAT (eds) Proceedings of Refraction of Transatmospheric signals in Geodesy, vol 36, Netherlands Geodetic Commission Publications on Geodesy, p 157–164.

Nilsson T, Böhm J, Wijaya DD, Tresch A, Nafisi V, Schuh H (2013) Atmospheric Effects in Space Geodesy, Springer Berlin Heidelberg, Berlin, Heidelberg, chap Path Delays in the Neutral Atmosphere, pp 73--136.

Nilsson T, Soja B, Karbon M, Heinkelmann R, Schuh H (2015) Application of Kalman filtering in VLBI data analysis. Earth, Planets and Space 67(1):1–9.

Petit G, Luzum B (eds) (2010) IERS Conventions (2010), IERS Technical Note, vol 36. Verlag des BKG, Frankfurt am Main, Germany.

Schuh H, Behrend D (2012) VLBI: A fascinating technique for geodesy and astrometry. J Geodyn 61:68–80.

Soja B, with eight co-authors (2015) Tropospheric delay determination by Kalman filtering VLBI data. Earth, Planets and Space 67(144):1–16.

Thayer GD (1974) An improved equation for the radio refractive index of air. Radio Sci 9(10):803–807.

Zus F, with six co-authors (2012) A methodology to compute GPS slant total delays in a numerical weather model. Radio Sci 47(2).